UCRL-JC-133915
PREPRINT

Work-Op IV Summary: Lessons from Iron Opacities

F. J. D. Serduke, E. Minguez, S. J. Davidson,
C. A. Iglesias

This paper was prepared for submittal to the
Radiative Properties of Hot Dense Matter
Sarasota, FL
October 26-30, 1998

April 16, 1999

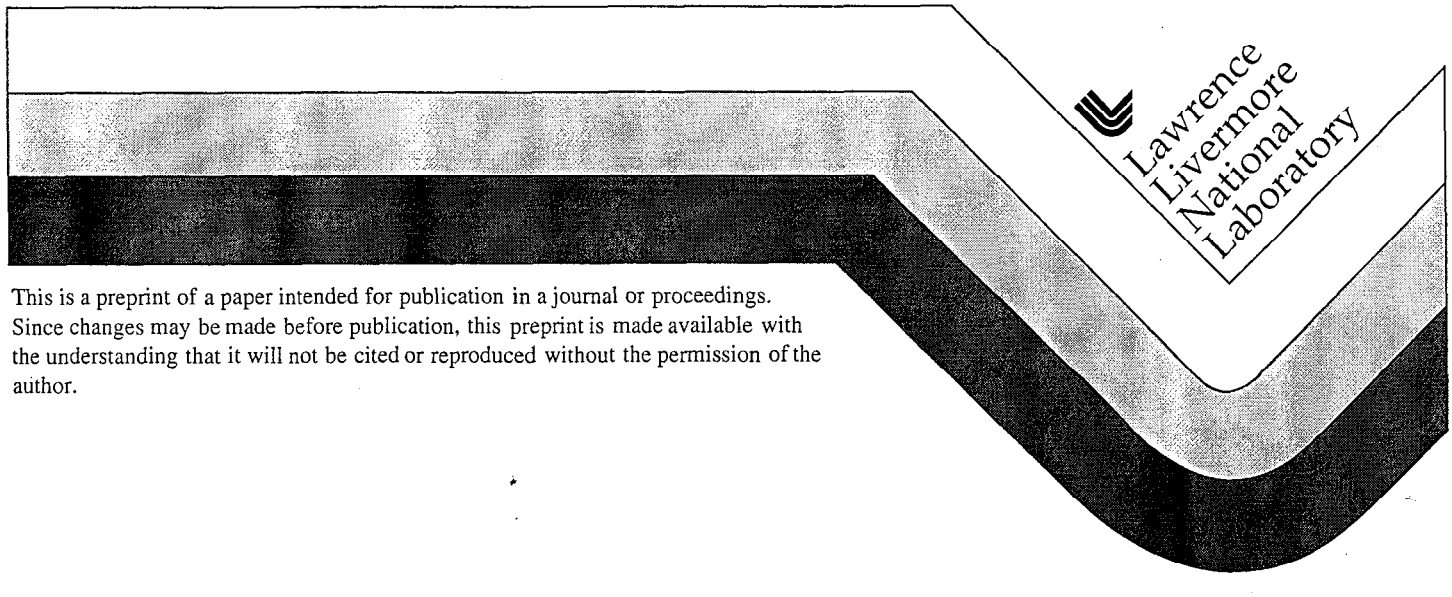

Work-Op IV Summary: Lessons from Iron Opacities

FRANKLIN J. D. SERDUKE[1], EMILIO MINGUEZ[2],
STEVEN J. DAVIDSON[3], and CARLOS A. IGLESIAS[1]
[1] Lawrence Livermore National Laboratory, Livermore, CA USA
[2] Institute for Nuclear Fusion, Polytechnical University of Madrid, Madrid, Spain
[3] AWE Aldermaston, Aldermaston, UK

The fourth international LTE opacity workshop and code comparison study, WorkOp-IV, was held in Madrid in 1997. Results of this workshop are summarized with a focus on iron opacities. In particular, the astrophysically important photon absorption region between 50 and 80 eV is emphasized for a sequence of iron plasmas at densities and temperatures that produce nearly the same average ionization stage (Z^*~8.6). Experimental data that addressed this spectral region is also reviewed.

I. Introduction

Computer models to calculate photon absorption coefficients for astrophysics, laser-created plasmas, inertial confinement fusion, and other applications have been under development for many decades. The pace of these developments has accelerated over the past ten years. The WorkOp series of opacity workshops (conceived by Frank Serduke in collaboration with Carlos Iglesias in 1988) has been helpful to this acceleration. The list of workshops, the hosts and host institutions are summarized in Table 1.

In this note, we give an overview of WorkOp-IV and present a summary description of the plasma cases studied. For the remainder of this article, we focus on a subset of the cases and use the unique opportunity of having calculations from over a dozen opacity codes to present some observations on the status of opacity modeling and on an important recent experiment.

The format of these workshops is the following:
1) Suggestions for cases to be studied are solicited from all potential participants. From these, the set of plasmas to be studied is specified by the organizing committee, about six months prior to the workshop. Case selection is itself a many-month process and is critical to the success of the workshop.
2) Calculations are submitted electronically, in a common format, about two months prior to the actual workshop. Participation in the workshop is generally limited to those who contribute code results.
3) Participants receive plots and interactive graphics files 3-4 weeks prior to the meeting giving them an opportunity to compare their own results with those of others before the workshop convenes.
4) The workshop is organized into moderated sessions that address subsets of the cases with the aid of Igor interactive graphics. Speakers are invited to present talks on developments in experiments, theory, and applications.
5) Preparation of the final report[1] involves an opportunity for participants to resubmit or withdraw their case contributions. The resubmission rate has generally been about 50%.

Results of previous WorkOps have been summarized at earlier RPHDM meetings by their hosts[2,3].

II. WorkOp-IV in Madrid

The Fourth International Opacity Workshop and Code Comparison Study, WorkOp-IV, convened at the Institute for Nuclear Fusion in Madrid of the Polytechnical University in Madrid, Spain in May of 1997. Our hosts were Dr. E. Minguez, Dr. G. Velarde and Dr. M. Velarde. There were about 20 codes that submitted calculations to this workshop. The list of participating codes together with the authors and the institutional affiliation of the principal author is presented in Table 2.

The Madrid workshop also had four invited presentations on topics of high interest to those in attendance. These are listed in Table 3.

There were 50 plasma cases specified for calculation; each case was defined by its temperature, density and composition. A major emphasis in case selection was on iron plasmas since all codes can address this element and there has been good success in studying iron during all previous workshops. We looked at a sequence of four iron plasmas that have nearly the same average ionization, $Z^*\sim 8.6$, ranging in density from 10^{-5} to 10^{-2} g/cm^3 and in temperature from 16 to 32 eV. There was an isothermal (100 eV) sequence of iron plasmas whose density spanned 10^{-4} g/cm^3 to 50 g/cm^3. A sequence at a constant density of 0.1 g/cm^3 with temperatures ranging from 20 eV to 1 keV was also included.

A selection of high density, low temperature plasmas was addressed; codes generally disagree under these plasma conditions. We also looked at mixtures; included among these were weakly and strongly coupled C_4Fe mixtures as well as some mixtures that have the material properties of foam. Another region of emphasis was the ablator of large-laser ICF ignition capsules; sequences of four plasmas each for brominated plastic and copper-doped beryllium that spanned the range of ablator conditions found just prior to ignition were addressed[4]. We revisited hydrogen at 1 eV and 10^{-6} g/cm^3 to look especially at line shapes since in this case line wings determine the Rosseland mean. Several aluminum cases were also considered. Cold and low temperature holmium were studied. We attempted to compute a number of new experiments but difficulties in specifying, with sufficient accuracy, the experimental conditions prior to the full analysis of the data made valid detailed comparisons difficult. A full list of the cases may be found in the final report[1] for WorkOp-IV.

III. Opacity of Iron Plasmas

Iron makes interesting case studies. It has sufficient complexity to be reasonably approximated by statistical techniques such as those using Unresolved-Transition-Array (UTA) or Super-Transition-Array (STA) approaches, yet is tractable by detailed term accounting (DTA) models. We present several comparisons of iron plasma calculations that address the differences between these two types of models.

Figure 1 illustrates various features of the spectroscopy and opacity of iron plasmas. The shaded area in the lower-left portion of the figure indicates where the opacity of iron is dominated by spectral lines. Moving to higher densities in this line-dominated region, results from statistical models and DTA models converge. Outside of this region, it is the continuum features and not the bound-bound absorption that dominate of the Rosseland mean opacity. Continuum lowering becomes important at higher densities; the area where the maximum bound orbital is the 6s and 3s is indicated by the long-dashed lines. There are regions near closed shells where bound-bound absorption features are reduced to a relatively small number of narrow lines. The trajectories, in this density-temperature space of empty 2s and empty 3s orbitals, are indicated by the solid black lines. The density-temperature positions of the WorkOp-IV cases are shown as circles. The Z*~8.6 sequence straddles a temperature of 20 eV at the bottom of the plot. The 100 eV isothermal sequence sits above the middle of the Line Dominated region. As we will see shortly, the participating codes had the largest variance in Rosseland mean opacity for the very low-density plasmas. There were also significant differences in mean ionization for the highest density case, 50 gm/cm^3.

III.1 Expressions for Mean Opacities

We will be discussing mean opacities in further detail. These were calculated using the expressions presented in equations 1 through 5. The normalized Planck Function may be written

$$B(\nu,T) = [15/(\pi^4 T)]\ u^3 / (e^u - 1) \qquad (1)$$

where the dimensionless variable $u = h\nu/T$, $h\nu$ is the photon energy and T is the temperature in energy units. The partial derivative of B with respect to T appears in the integrand of the Rosseland mean.

$$B'(\nu,T) = \partial B(\nu,T) / \partial T = [15/(4\pi^4 T)]\ u^4 e^u / (e^u - 1)^2. \qquad (2)$$

B and B' are smooth, slowly varying functions that peak at about 3 kT and 4 kT respectively. Both B and B' are normalized so that

$$\int_0^\infty d\nu\ B(\nu,T) = \int_0^\infty d\nu\ B'(\nu,T) = 1. \qquad (3)$$

The Rosseland Mean Opacity is a weighted harmonic mean

$$1/\kappa_{Rosseland}(\rho,T) = \int_0^\infty d\nu\ B'(\nu,T) / \kappa_{total}(\rho,T,\nu), \qquad (4)$$

and the Planck Mean Opacity is a weighted mean

$$\kappa_{Planck}(\rho,T) = \int_0^\infty d\nu\ B(\nu,T)\ [\kappa_{total}(\rho,T,\nu) - \kappa_{scattering}(\rho,T,\nu)]. \qquad (5)$$

where κ_{total} is the total absorption coefficient including the bound-bound, bound-free, free-free and scattering contributions; it depends on the plasma density ρ and temperature T, as well as on the photon energy $h\nu$.

III.2 Iron Mean Opacities

A bird's-eye view of the workshop mean opacities for iron is presented in Figs. 2, 3, and 4.

Mean opacities are plotted vs. code name and grouped by plasma case; the plasma conditions are noted for each grouping on these plots.

The opacities plotted are the Rosseland Mean (solid triangles), Planck Mean (open circles), and the continuous Rosseland Mean (small open triangles). The continuous Rosseland Mean includes the bound-free, the free-free, and scattering contributions to the total opacity and excludes the bound-bound contribution. The importance of bound-bound absorption to the Rosseland Mean is indicated by the difference between the Rosseland Mean and the continuous Rosseland Mean. Differences in the Rosseland and Planck Means reflect the differences between the peaks and the valleys of $\kappa_{total}(\rho,T,\nu)$. If κ_{total} were a constant, the Rosseland and Planck means would be identical (except for the scattering contribution, which is usually negligible). The height of the Rosseland Mean filled-triangle plot symbol spans about ±10% about the calculated opacity. A large variance among the code predictions is indicated for cases where the large triangles "dance". If the triangles were to line up, the codes agree.

It is evident from Figs. 2-4 that the largest percentage variances among the code results for these iron cases are found at low densities. Agreement improves as a density of 0.1 g/cm^3 is approached but then tends to degrade a bit at higher density.

How close an agreement is good enough? Unfortunately, the answer depends closely upon the application. For example, in the solar core, a 1% opacity change leads to qualitative changes in solar model predictions. For variable Cepheids, 10%-20% opacity agreement is presently satisfactory for stellar pulsation.

III.3 Opacity of the 3-3 bump between 50 and 80 eV

Iron is an important component of astrophysical plasmas. In this section, we will focus on the M-shell $\Delta n=0$ (3-3) transition array in the Z*~8.6 sequence of iron cases. Iron at 20 eV, 10^{-4} g/cm^3 has been a case in all the WorkOps and is associated with the important problem of modeling the pulsation properties of variable Cepheid stars. It must be noted that in a pure iron plasma, the Rosseland Mean Opacity is governed by the depth of the wings of this transition array and not by its central porosity to radiation flow. However, in astrophysical mixtures, the situation changes as the dominant hydrogen and helium components fill in the wings of the iron $\Delta n=0$ bump making the porosity of the central part of the bump important.

The temperature of the Z*~8.6 sequence of iron cases increases with increasing density. This sequence has transition arrays that are nominally produced by configurations with the same total numbers of bound electrons. Of course as we progress to higher densities through this Z*~8.6 sequence, there is a large change in the electron density in which the ion is immersed with consequent effects on spectral line shapes, bound electron fluctuations and line merging.

Because the Rosseland weighting factor depends of temperature (see eq. 4) and we would like to use the same weighting function for all members of the Z*~8.6 sequence, we choose to represent the "porosity" of the bump by introducing a harmonic bump opacity

$$1/\kappa_{Bump} = \int_{50\,eV}^{80\,eV} d\nu \; / \; [Base + \kappa(\nu)], \qquad (6)$$

where Base, which equals 10^4 cm^2/g, simulates the effect of the hydrogen-helium background and where both the total opacity and the bound-bound opacity have been used separately for $\kappa(\nu)$. Note that the bump opacity is only integrated from 50 eV to 80 eV. This harmonic mean crudely simulates one of the major features of some astrophysical mixtures.

The bound-bound opacity for a variety of the participating codes is illustrated in Fig. 5. For clarity, the bound-bound opacities in Fig. 5 has been multiplied by a factor of ten for each factor of ten increase in the density above 10^{-5} g/cm^3. The lowest plotted $\kappa_{Bound\text{-}Bound}$ is for 10^{-5} g/cm^3. The highest plotted $\kappa_{Bound\text{-}Bound}$ is 10^3 x $\kappa_{Bound\text{-}Bound}$ for 10^{-2} g/cm^3. The variance of the magnitude of the line structure shown for the DTA codes, LEDCOP and OPAL, decreases markedly with increasing density even though the ionization states that contribute change relatively little. All codes exhibit a reduction in the depths of the wings of the transition arrays with increasing density. The widths of the transition arrays are also seen not to be the same for all of the models.

The κ_{total} and $\kappa_{bound\text{-}bound}$ bump opacities for each code that submitted calculations for this entire Z*~8.6 sequence are grouped together and displayed in Fig. 6. This is a linear plot starting at 10^4 cm^2/gm, which is by definition, the lowest possible value for κ_{Bump}.

There appear to be two classes of results:
1) codes for which the bump opacity is only weakly dependent on density,
2) codes that exhibit a strong density dependence from 10^{-5} to 10^{-3} g/cm^3.

The experiment of Springer *et al.*[6] strongly suggests, for iron plasmas in the vicinity of 20 eV and 10^{-4} g/cm^3, the existence of discrete line structure (porosity) in the iron transition arrays that so far appears to be addressable only by DTA opacity models. For the 50 to 80 eV bump at densities below 10^{-3} g/cm^3, the results suggest that codes approximating transition arrays by broad structures may only get the bump opacity (and by implication astrophysical opacities) correct at a limited range of densities.

IV. Experiments

Experiments have been extremely important to the development and validation of opacity models. A significant number of useful experiments have been performed over the past decade and have served to test, in some manner, virtually all of today's sophisticated opacity codes.

As with all previous WorkOps, we included cases that addressed recent experiments. For many of these cases, the data were in early stages of analysis. Unfortunately, the final conditions of the experiments turned out to be significantly different from the conditions requested of WorkOp participants; thus it is not possible to present detailed comparisons of theoretical predictions of experimentally measured x-ray transmission or emission.

Furthermore, for some of these experiments, uniformity of the temperature and density of the plasma was an issue; this subject has been discussed by Perry *et al.*[7].

The iron experiment performed by Springer *et al.*[6] studied opacities for stellar envelopes by measuring x-ray transmission in the vicinity of the M-shell $\Delta n=0$ bump discussed above. This was an important first step in a new class of opacity experiments. LTE plasma conditions were achieved in the laboratory that had not been approached previously. The long-duration Planckian radiation field that heated the sample uniformly to close to 20 eV, the low plasma density (10^{-4} g/cm^3), and the good resolving power ($E/\Delta E > 2000$) were all impressive. Although it was stated that x-ray transmission through two lengths, 10 mm and 2 mm, of 10^{-4} g/cm^3 plasma were measured, only the 10 mm results were reported[6] in the sole published account of this experiment.

We present calculational results, in Fig. 7, for transmission through a pure iron plasma, 10 mm long at 20 eV and 10^{-4} g/cm^3. Two codes were selected: LEDCOP as a representative of DTA codes and STA as a representative of UTA codes. Transmission results that appear above the experimental data have been convolved with a gaussian whose full-width at half maximum is the stated experimental resolution; those beneath have not. The separation of tick marks on the Transmission axis is 25%.

The conditions of the experiment may potentially be different from those of the 20 eV, 10^{-4} g/cm^3 of the calculations. For example, the temperature was possibly several eV away from 20 eV and there was significant oxygen contamination of the sample affecting the electron density by as much as 20%. In addition, experimental details such as background subtraction and higher-order crystal diffraction are known to be problems in other plasma transmission experiments. It would be important to know how these were addressed here. The experiment presents compelling evidence of the need for detailed-line accounting in modeling iron plasmas of this density and temperature. The photon energy and profile of the high-energy side of the bump is measured by the experiment which represents an advance as its location and shape presents difficulties for several opacity models.

IV.1 Need for More Experiments

The opacity community in general and the workshops have benefited greatly from the experimental data provided. Experiments provide crucial, independent tests of the opacity codes as well as an impetus for further theoretical developments.

Although the Springer *et al.*[6] iron measurement described made a substantial contribution to opacity research, further development of such experiments would be valued and is encouraged. In particular, we would suggest the following:

1) The width of the $\Delta n=0$ bump remains an outstanding issue to be experimentally addressed. This would require an extension of the measured spectral region to photon energies below 60 eV.

2) The astrophysically important structure of the central region of the $\Delta n=0$ bump should be addressed experimentally by use of a significantly thinner sample. This was already done but not yet reported by Springer *et al.*[6] with of a 2 mm sample that would be expected to exhibit-

very little saturation of the transmission in this spectral region.
3) Simultaneous measurements of transmission through samples of two different thicknesses may be used to check many aspects of the data[5] such as saturation effects, the presence of unresolved structure, and data reduction difficulties involving sample emission. Experience has shown that this can be a very sensitive test of the fidelity of x-ray film processing, background subtraction, and assumptions about the uniformity of the sample.

In short, the further development of experimental techniques and their application to a wide range of opacity problems is not only welcomed but essential for continuing progress in the field.

V. Conclusions

These LTE opacity workshops have been a valuable tool to both code developers and users of opacities. WorkOps I through IV have coincided with and have served as a significant calculational testing ground for major advances in the state of the art. A full presentation of the contributions to the WorkOp is beyond the scope of this paper but may be found in the final report[1].

In WorkOp-IV, we have found or reconfirmed several aspects of opacity modeling:
• High densities at low temperatures pose major computational difficulties for codes. This is manifested in ionization balance as well as opacity.
• Iron (Z=26) provides important test cases as the two major competing approaches, statistical methods and DTA methods, are both applicable to the modeling of iron.
• Near 20 eV and for densities of 0.001 g/cm^3 or higher, DTA and UTA tend to agree on the computed Rosseland mean opacity. However, at 20 eV and a density of 10^{-4} g/cm^3 or lower, the porosity of transition arrays predicted by DTA models and supported by experiment, is not well represented by statistical treatments.
• The above mentioned difference in the porosity has implications for stellar pulsation models. The Rosseland mean opacities for pure iron may agree for DTA and UTA models because it is determined by the wings of the bump, not the wings of the individual line transitions. But when iron appears in an astrophysical mixture at the same electron density, it is the porosity of the central part of the bump, determined by the shapes of myriad lines, that governs its contribution to the mixture opacity; the wings of the bump are filled by the dominant hydrogen and helium components of the mixture.
• Experiments, although difficult, are essential to further progress in the understanding and modeling of opacities. Comparisons of experimental results with several calculations show that numerous issues remain to be addressed.

References:

1. Serduke, Franklin and Minguez, Emilio Final Report on WorkOp-IV:97, University of California Lawrence Livermore National Laboratory Internal Report (unpublished)

2. Rose, S. J. *JQSRT* **51**, 317 (1994)

3. Rickert, A. *JQSRT* **54**, 325 (1995)

4. Haan, Steve, LLNL, private communication (1997)

5. Perry, T. S., Davidson, S. J., Serduke, F. J. D., Bach, D. R., Smith, C. C., Foster, J. M., Doyas, R. J., Ward, R. A., Iglesias, C. A., Rogers, F. J., Abdallah, Jr., J., Stewart, R. E., Kilkenny, J. D., and Lee, R. W., *Phys. Rev. Lett.* **67,** 3784 (1991)

6. Springer, P. T., Wong, K. L., Iglesias, C. A., Hammer, J. H., Porter, J. L., Toor, A., Goldstein, W. H., Wilson, B. G., Rogers, F. J., Deeney, C., Dearborn, D. S., Bruns, C., Emig, J., and Stewart, R. E., *JQSRT* **58**, 927 (1997)

7. Perry, T. S., Springer, P. T., Fields, D. F., Bach, D. R., Serduke, F. J. D., Iglesias, C. A., Rogers, F. J., Nash, J. K., Chen, M. H., Wilson, B. G., Goldstein, W. H., Rozsnyai, B., Ward, R. A., Kilkenny, J. D., Doyas, R., Da Silva, L. B., Back, C. A., Cauble, R., Davidson, S. J., Foster, J. M., Smith, C. C., Bar-Shalom, A., Lee, R. W., *Phys. Rev. E* **54**, 5617 (1996).

*This work was performed under the auspices of the U.S. Department of Energy by Lawrence Livermore National Laboratory under contract No. W-7405-Eng-48.

WorkOp	Host(s)	Host Institution	Location
I-1989	S. Rose, S. Davidson, J. Foster, C. Smith	Rutherford Appleton Laboratory	RAL, UK
II-1991	J. Lachkar, G. Dammame, M. Vuillemin	CEA Limeil-Valenton	Orsay, France
III-1994	A. Rickert, K. Eidmann, J. Meyer-ter-Vehn	Max Planck Institute for Quantum Optics	Garching, Germany
IV-1997	E. Minguez, G. Velarde, M. Velarde	Institute for Nuclear Fusion, Polytechnical University of Madrid	Madrid, Spain
V-2000	S. Davidson, B. Crowley	AWE , Aldermaston	Oxford, UK

Table 1. History and immediate future of the International LTE Opacity workshops

CODE	AUTHORS	Institution
AGPR	F. Perrot, A. Grimaldi	CEA-LV
ANALOP	J.M. Gil, J.G. Rubiano, P. Martel, L. Doreste, E. Minguez	ULPGC-UPM
CASSANDRA	B. Crowley, S. Davidson, D. Landeg, D. Rowley	AWE
CORONA	T. Nishikawa	OKAYAMA U.
FINE	D. Kilcrease, J. Abdallah, R.E.H. Clark	LANL
HEO-II	J.J. Keady, D. Kilcrease, J. Abdallah, C. Fontes	LANL
HOPE	B. Rozsnyai	LLNL
IMP	S. Rose	RAL
JIMENA	E. Minguez	IFN-UPM
LEDCOP	N. Magee, A.L. Merts, J.J. Keady, D.P. Kilcrease	LANL
OPAL	C.A. Iglesias, F.J. Rogers, B.G. Wilson	LLNL
OPA-LV	P. Dallot, M. Busquet, R. Chirat, G. Dejonghe, A. Grimaldi, P. Kaiser, F. Perrot, J.P. Raucourt, M. Vuillemin, M. Zembri	CEA-LV
OPINCH	X. Meng, Y. Sun	IAPCM
POTREC	J.C. Gauthier, A. Mirone, F. Gilleron, C. Chenais Popovics	LULI
SCO	T. Blenski, F. Perrot, A. Grimaldi	LULI
SHOP	G. Faussurier	CEA-LV
SHOPZ	G. Faussurier	CEA-LV
STA	A. Bar-Shalom, J. Oreg, W.H. Goldstein	BEN-GURION U.
THERMOS	A. Nikiforov, V.G. Novikov, A.D. Solomyannaya	KELDYSH INST.

Table 2. Codes whose authors participated in WorkOp-IV. All code authors are shown; most attended.

Invited Speakers	Affiliation	Topic
Jacques Bauche and Claire Bauche-Arnoult	Laboratoire Aime Cotton	Transition Arrays
Klaus Eidmann	MPQ - Garching	Laser Experiments
Marcel Klapisch	Naval Research Laboratory	New Directions in Opacity Modeling
Paul Springer	Lawrence Livermore National Laboratory	Opacity Experiments of Astrophysical Relevance

Table 3. Invited speakers at WorkOp-IV.

Figure Captions.

1. A density-temperature plot of interesting features of the opacity and spectroscopy of iron. A filled circle indicates the density-temperature coordinate of a test case that was addressed in WorkOp-IV.

2. A graphical table of the mean opacities of the Z*~8.6 sequence of iron cases. Three mean opacities are plotted versus code name and grouped by case. The opacities plotted are the Rosseland Mean (solid triangles), the Planck mean (open circles) and the Continuous Rosseland Mean (small open triangles). The difference between the open and solid triangles is an indication of the importance of the bound-bound opacity to the overall Rosseland Mean.

3. A graphical table of the mean opacities of the lower-density part of the 100 eV isothermal sequence of iron cases. See the figure 2 caption for more information.

4. A graphical table of the mean opacities of the higher-density part of the 100 eV isothermal sequence of iron cases. See the figure 2 caption for more information.

5. A plot of the bound-bound opacity of the Z*~8.6 iron sequence for a subset of the codes that participated. The four plots are for densities ranging from 10^{-5} to 10^{-2} g/cm^3. Separation of the plots was achieved by multiplication of the opacity by a factor of ten for each increase in a factor of ten in density.

6. A graphical table plot of the bump opacity that is defined in eq. 6. Calculations are grouped by code for all four members of the Z*~8.6 sequence.

7. A plot of the 10 mm x-ray transmission experiment of Springer *et al.*[6] which was nominally performed for iron at 20 eV at a density of 10^{-4} g/cm^3. Actual conditions differed somewhat as discussed in ref. 6 and in the text. We also present, at the nominal conditions, calculated x-ray transmission for LEDCOP as a representative DTA code and STA as a representative UTA code. Theoretical results for LEDCOP and STA that appear above the experimental results have been convolved with the instrumental resolution of the experiment. The LEDCOP plot beneath the experimental data has not been smoothed by the experimental resolution. Tick marks on the transmission axis are separated by 25%.

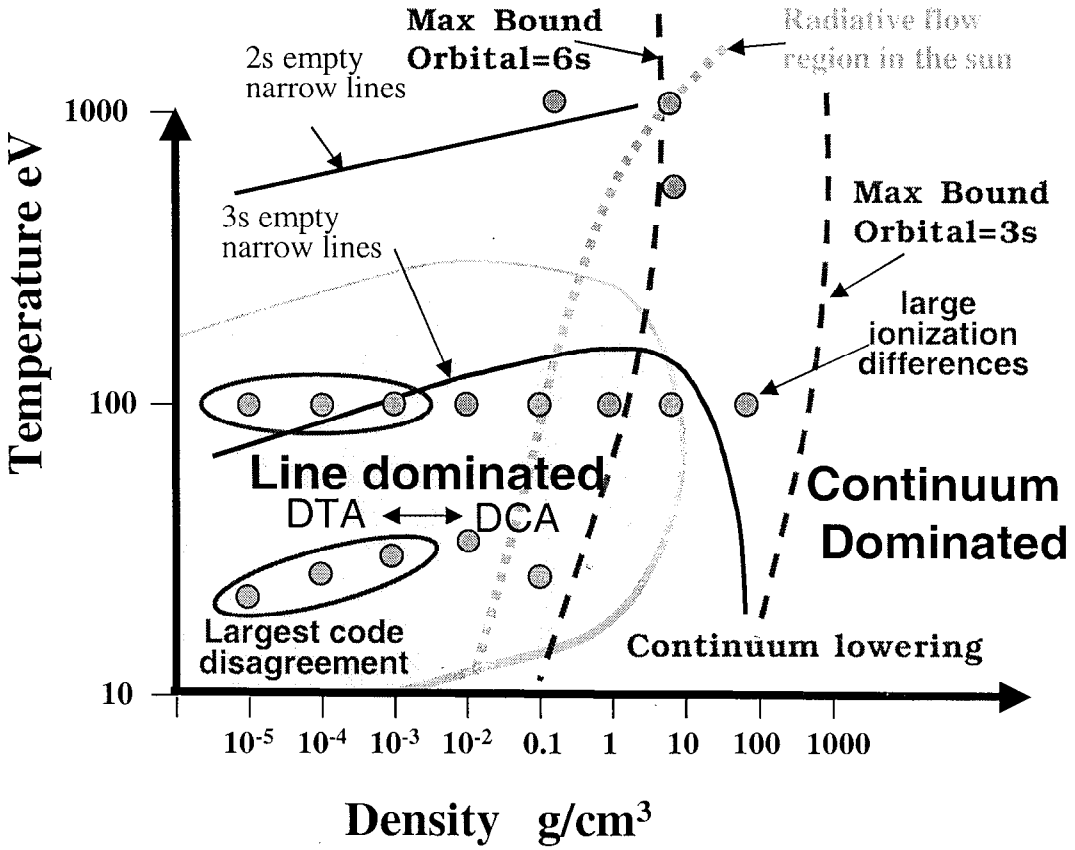
Max Bound
Orbital=6s
Radiative flow
region in the sun
2s empty
narrow lines
1000
Temperature eV
3s empty
narrow lines
Max Bound
Orbital=3s
large
ionization
differences
100
Line dominated
DTA ↔ DCA
Continuum
Dominated
Largest code
disagreement
Continuum lowering
10
10-5 10-4 10-3 10-2 0.1 1 10 100 1000
Density g/cm3

Figure 1

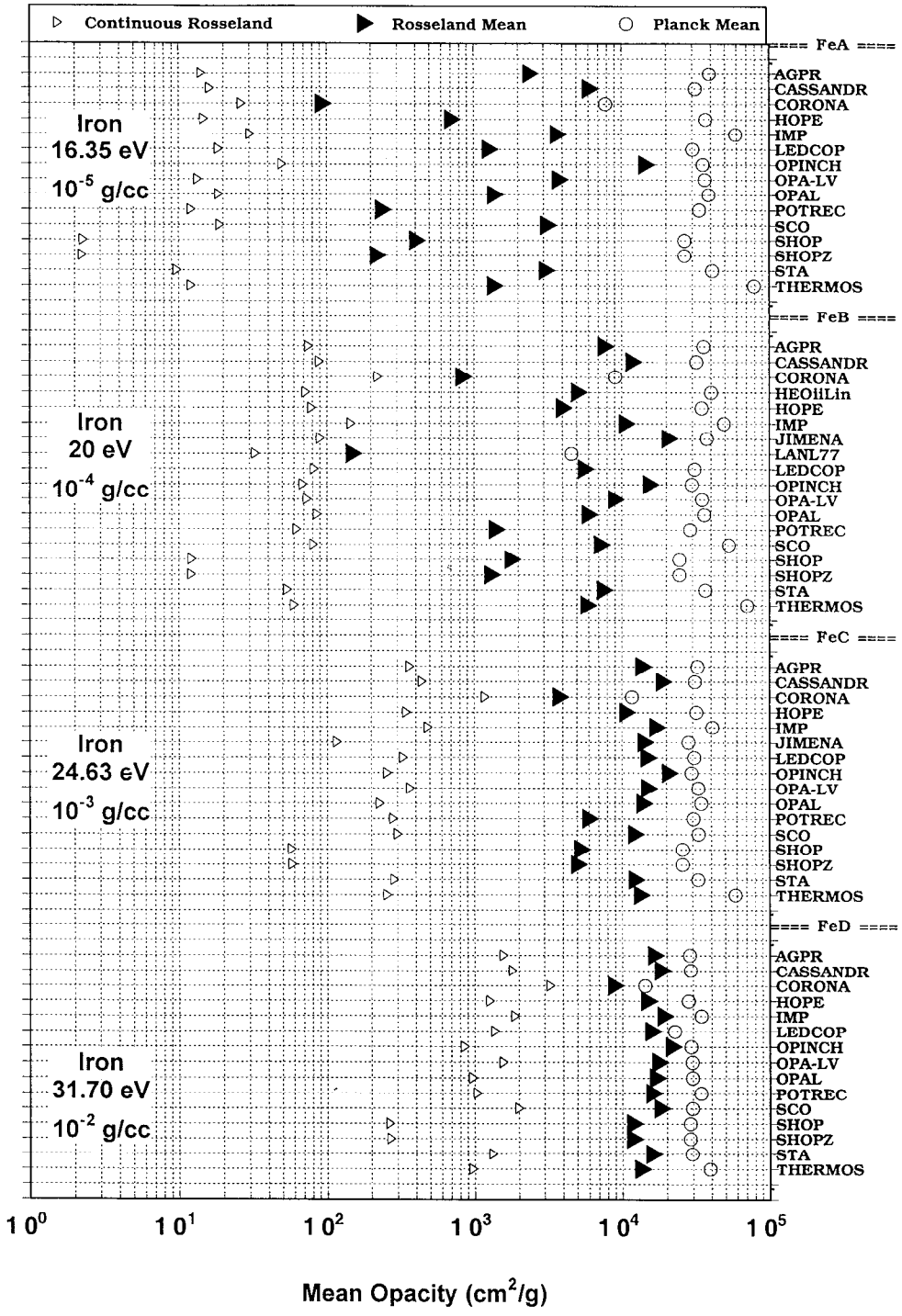
Continuous Rosseland
Rosseland Mean
Planck Mean
Iron
16.35 eV
10^-5 g/cc
Iron
20 eV
10^-4 g/cc
Iron
24.63 eV
10^-3 g/cc
Iron
31.70 eV
10^-2 g/cc
==== FeA ====
AGPR
CASSANDR
CORONA
HOPE
IMP
LEDCOP
OPINCH
OPA-LV
OPAL
POTREC
SCO
SHOP
SHOPZ
STA
THERMOS
==== FeB ====
AGPR
CASSANDR
CORONA
HEOliLin
HOPE
IMP
JIMENA
LANL77
LEDCOP
OPINCH
OPA-LV
OPAL
POTREC
SCO
SHOP
SHOPZ
STA
THERMOS
==== FeC ====
AGPR
CASSANDR
CORONA
HOPE
IMP
JIMENA
LEDCOP
OPINCH
OPA-LV
OPAL
POTREC
SCO
SHOP
SHOPZ
STA
THERMOS
==== FeD ====
AGPR
CASSANDR
CORONA
HOPE
IMP
LEDCOP
OPINCH
OPA-LV
OPAL
POTREC
SCO
SHOP
SHOPZ
STA
THERMOS
10^0
10^1
10^2
10^3
10^4
10^5
Mean Opacity (cm^2/g)

Figure 2

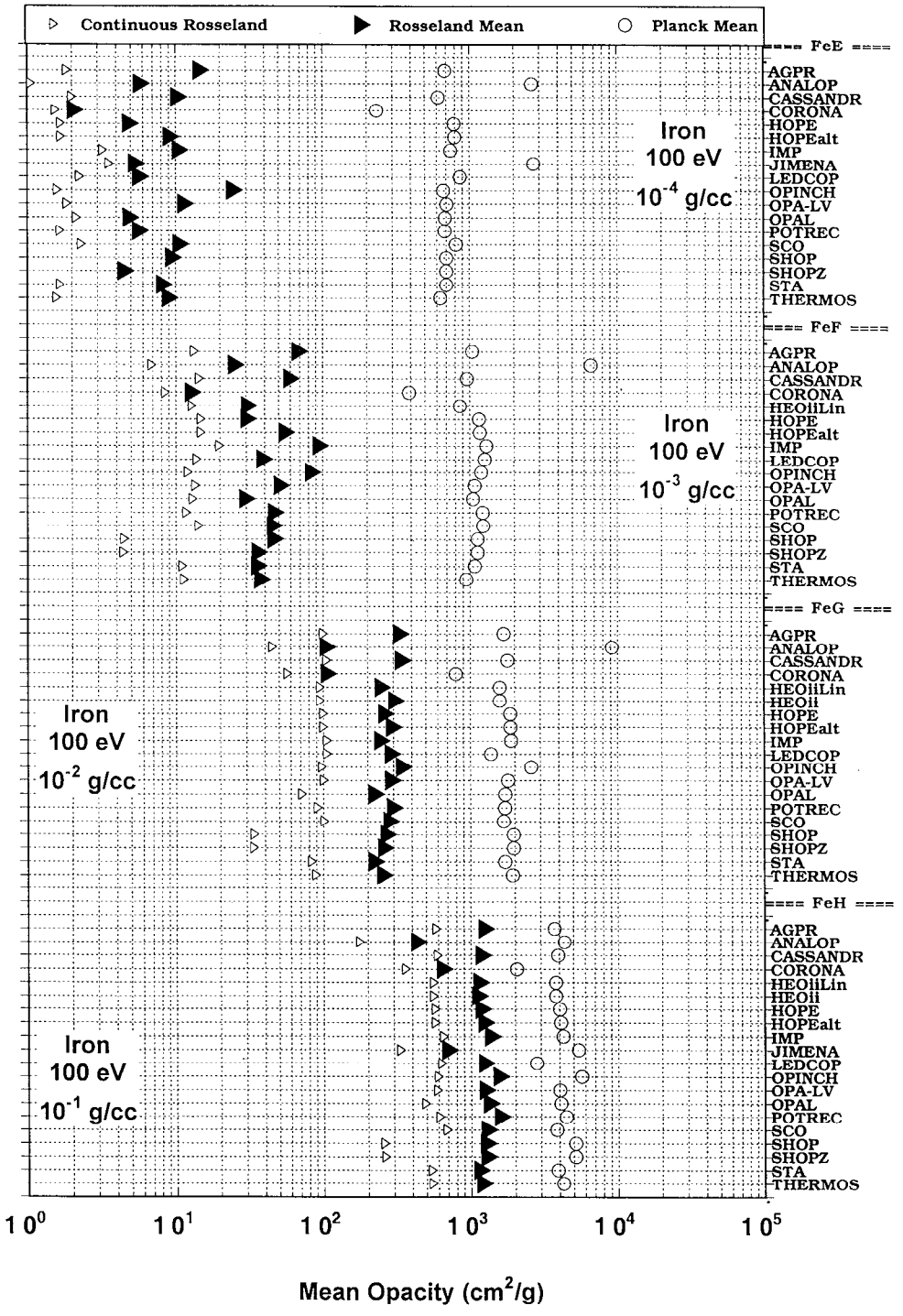
Continuous Rosseland
Rosseland Mean
Planck Mean
Iron
100 eV
10^-4 g/cc
Iron
100 eV
10^-3 g/cc
Iron
100 eV
10^-2 g/cc
Iron
100 eV
10^-1 g/cc
10^0
10^1
10^2
10^3
10^4
10^5
Mean Opacity (cm^2/g)
==== FeE ====
AGPR
ANALOP
CASSANDR
CORONA
HOPE
HOPEalt
IMP
JIMENA
LEDCOP
OPINCH
OPA-LV
OPAL
POTREC
SCO
SHOP
SHOPZ
STA
THERMOS
==== FeF ====
AGPR
ANALOP
CASSANDR
CORONA
HEOiiLin
HOPE
HOPEalt
IMP
LEDCOP
OPINCH
OPA-LV
OPAL
POTREC
SCO
SHOP
SHOPZ
STA
THERMOS
==== FeG ====
AGPR
ANALOP
CASSANDR
CORONA
HEOiiLin
HEOii
HOPE
HOPEalt
IMP
LEDCOP
OPINCH
OPA-LV
OPAL
POTREC
SCO
SHOP
SHOPZ
STA
THERMOS
==== FeH ====
AGPR
ANALOP
CASSANDR
CORONA
HEOiiLin
HEOii
HOPE
HOPEalt
IMP
JIMENA
LEDCOP
OPINCH
OPA-LV
OPAL
POTREC
SCO
SHOP
SHOPZ
STA
THERMOS

Figure 3

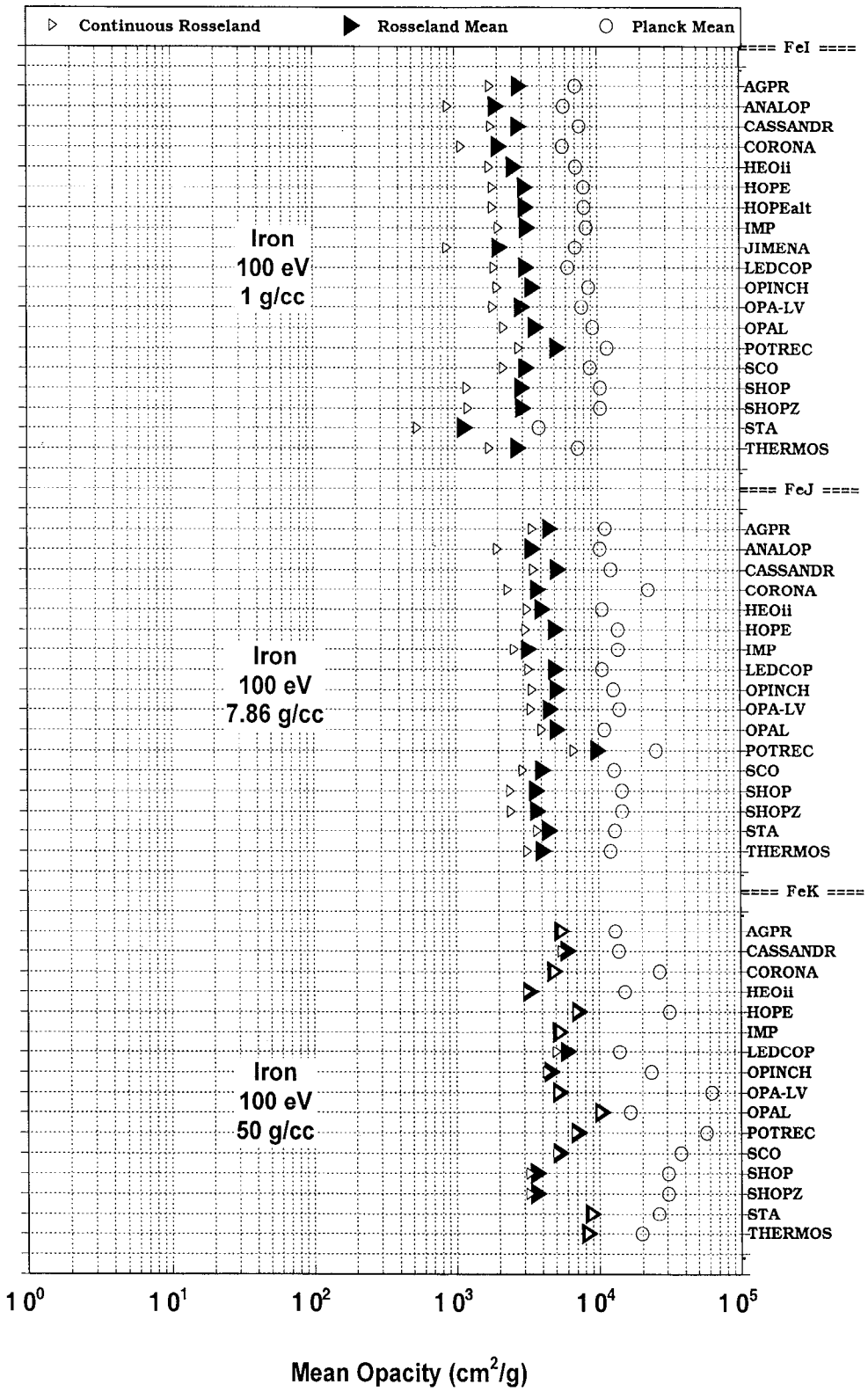
Continuous Rosseland
Rosseland Mean
Planck Mean
==== FeI ====
AGPR
ANALOP
CASSANDR
CORONA
HEOii
HOPE
HOPEalt
IMP
JIMENA
LEDCOP
OPINCH
OPA-LV
OPAL
POTREC
SCO
SHOP
SHOPZ
STA
THERMOS
Iron
100 eV
1 g/cc
==== FeJ ====
AGPR
ANALOP
CASSANDR
CORONA
HEOii
HOPE
IMP
LEDCOP
OPINCH
OPA-LV
OPAL
POTREC
SCO
SHOP
SHOPZ
STA
THERMOS
Iron
100 eV
7.86 g/cc
==== FeK ====
AGPR
CASSANDR
CORONA
HEOii
HOPE
IMP
LEDCOP
OPINCH
OPA-LV
OPAL
POTREC
SCO
SHOP
SHOPZ
STA
THERMOS
Iron
100 eV
50 g/cc
10^0
10^1
10^2
10^3
10^4
10^5
Mean Opacity (cm^2/g)

Figure 4

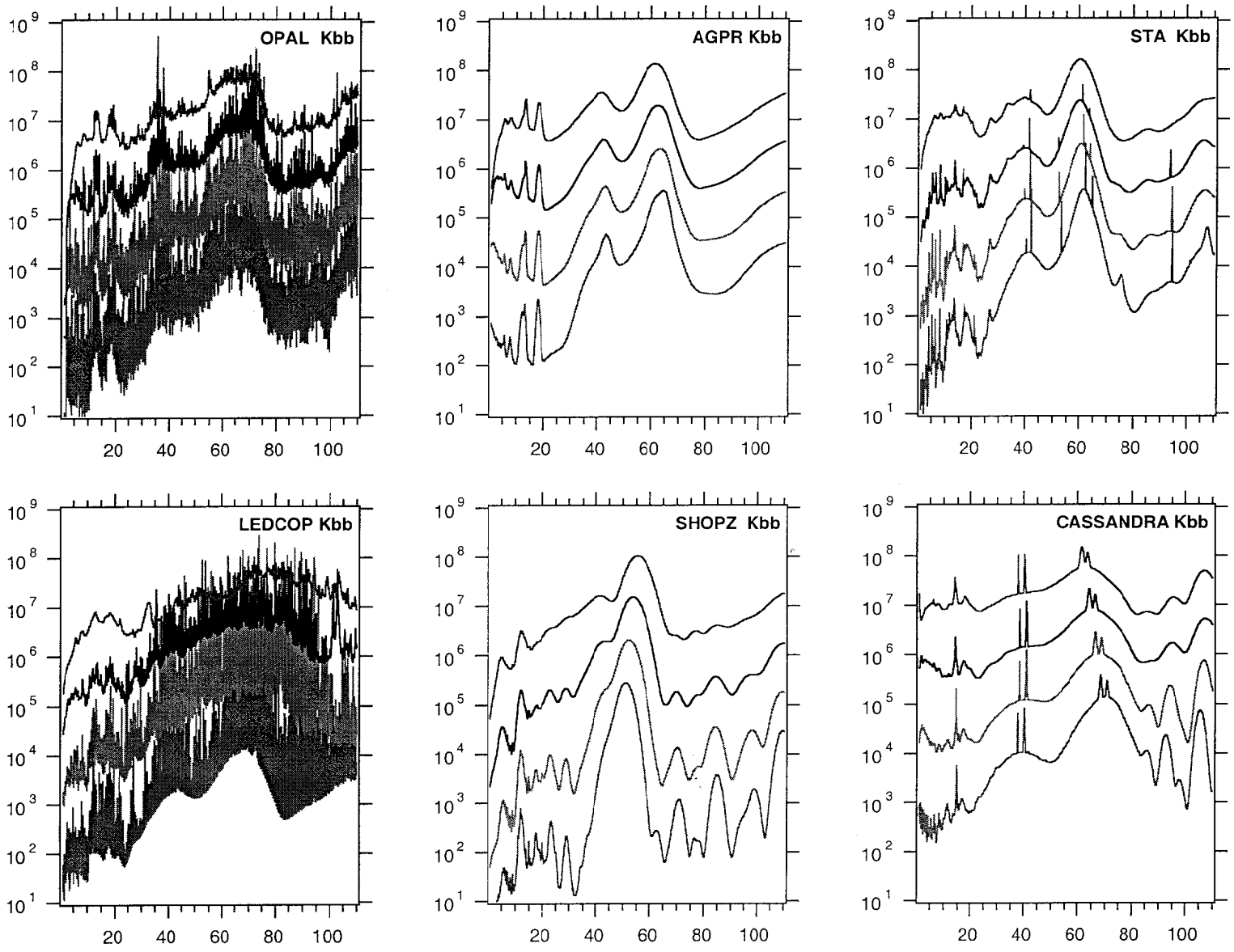
OPAL Kbb
AGPR Kbb
STA Kbb
LEDCOP Kbb
SHOPZ Kbb
CASSANDRA Kbb
10^9
10^8
10^7
10^6
10^5
10^4
10^3
10^2
10^1
20
40
60
80
100

Figure 5

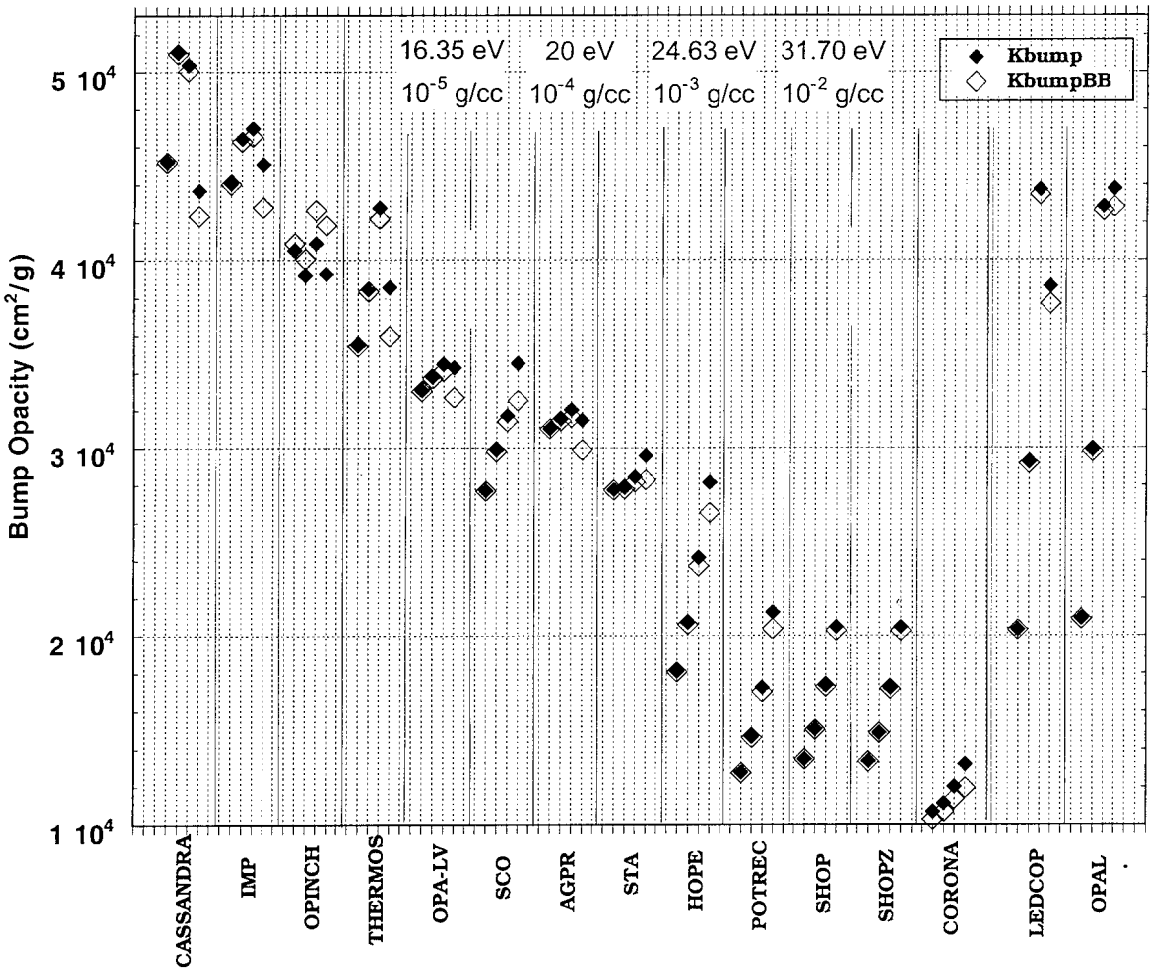
16.35 eV
10^-5 g/cc
20 eV
10^-4 g/cc
24.63 eV
10^-3 g/cc
31.70 eV
10^-2 g/cc
Kbump
KbumpBB
Bump Opacity (cm^2/g)
5 10^4
4 10^4
3 10^4
2 10^4
1 10^4
CASSANDRA
IMP
OPINCH
THERMOS
OPA-LV
SCO
AGPR
STA
HOPE
POTREC
SHOP
SHOPZ
CORONA
LEDCOP
OPAL

Figure 6

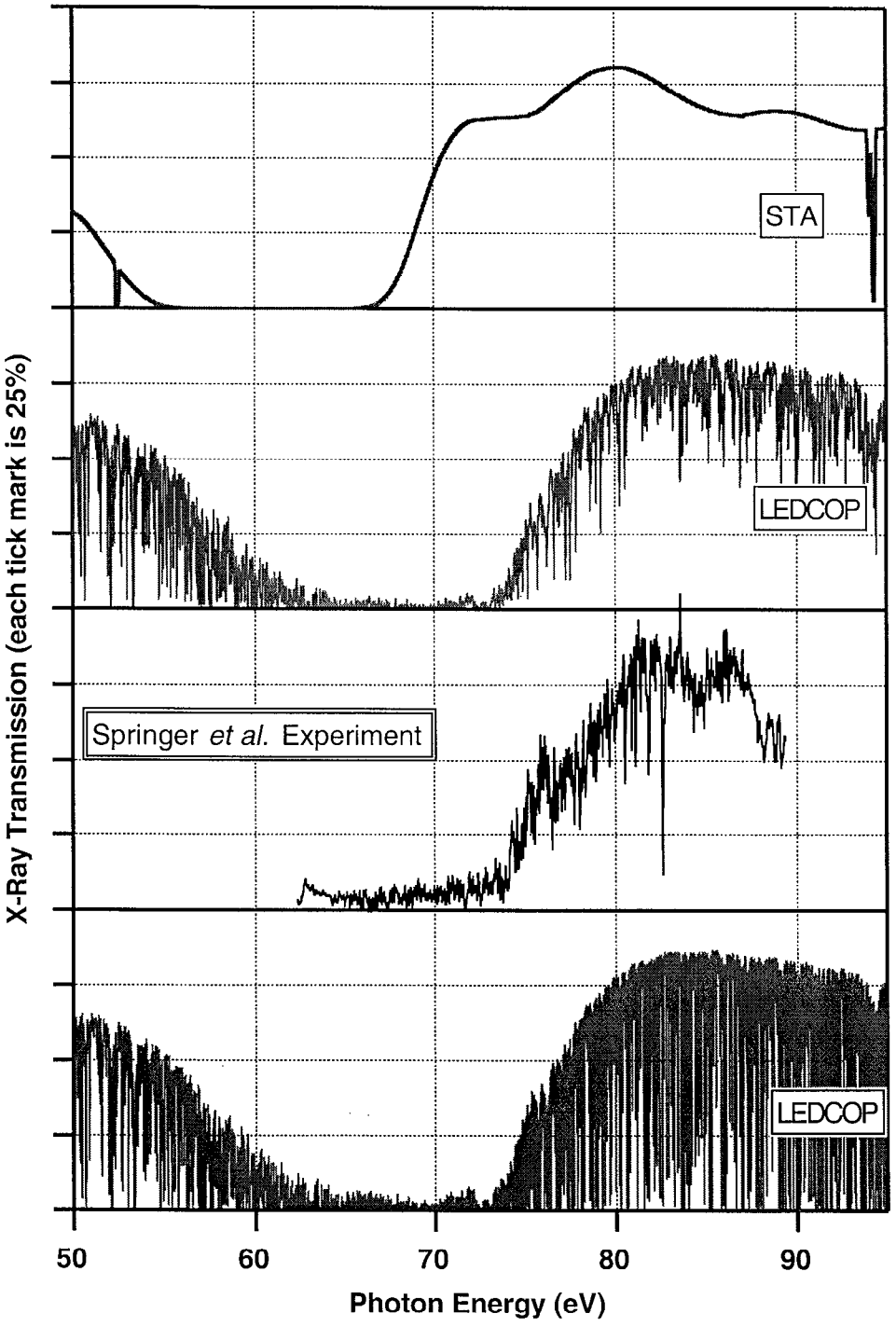
STA
LEDCOP
Springer *et al.* Experiment
LEDCOP
X-Ray Transmission (each tick mark is 25%)
50
60
70
80
90
Photon Energy (eV)

Figure 7